Mode Switching Algorithm to Improve Variable-Pitch-Propeller Thrust Generation for Drones Under Motor Current Limitation

Yuto Naoki, *Student Member, IEEE,* Sakahisa Nagai, *Member, IEEE,* Hiroshi Fujimoto, *Senior Member, IEEE*

***Abstract*—Research and development are active in multirotor drones. Attention has been focused on improving drone mobility performance by introducing variable pitch propellers. However, previous studies have not considered main motor currents in their controller design. The aim of this study is to improve thrust response by controlling the variable pitch propeller in the thrust dimension while keeping steady-state efficiency. Feed-forward control of thrust by switching modes using maximum current was designed. The control is designed to switch between a thrust reaching mode that uses pitch angle and rotational speed and a efficiency optimizing mode. The mode switching transitions were verified by simulation, and the effectiveness of the proposal was experimentally validated.**

***Index Terms*—variable pitch propeller, mode switching control, thrust control, current saturation.**

I. Introduction

RESEARCH and development in electric vertical take-off and landing (eVTOL) in multirotor types, including small UAVs and drones, have attracted attention owing to increased applications such as imaging, inspection, and transportation. One factor that has made the multirotor type mainstream and widespread is simplicity. Unlike the single-rotor type, the multirotor type has several propellers whose pitch is fixed, and only the rotational speed is controlled. Instead, the multiple rotors are controlled independently [1]. However, in the future, multirotor is expected to be used in large vehicles for industrial applications such as flying cars, which will require more sophisticated control [2]. Among these requirements, the key issues are improving their motion performance, efficiency, and flying range extension. Several approaches have been taken to improve mobility, such as adding degrees of freedom by fully-actuated UAVs [3], reducing the weight of the motor [4], and generating a trajectory that considers motor efficiency [5].

Variable pitch propellers are being studied to improve performance of the vehicles by adding degree of freedom (DoF) of mobility. Variable-pitch propellers have been used in propeller-driven aircraft and helicopters. Research on the application for electric aircraft has focused on the power consumption minimization control by optimizing the pitch angle and rotational speed [6], and regenerative energy optimization control [7]. The application of variable pitch propellers to drones has been studied out for its advantages in control aspects such as response [8] and energy aspects such as power consumption [9]. Variable pitch propellers have characteristics of an additional DoF in terms of pitch angle. It is possible to use the DoF to perform more stable emergency landings when the number of rotor degrees of freedom is reduced due to failure [10]. There is research on applying reversible thrust generation and unique airframe shapes to use the additional DoF [11], [12]. In the study of attitude and motion control of drones with variable pitch propellers, there are several methods such as PID control [8], nonlinear control using dynamic inversion [13], quaternion-based adaptive control [14], and robust control design [15].

In general drones, thrust is controlled only in the attitude dimension using a static aerodynamic model that relates rotational speed to thrust. However, controls have been developed that use a fixed-pitch propeller to estimate thrust and provide feedback control in thrust dimension [16]. In variable pitch propellers, the method can not be applied since the lift coefficient is time-varying. Nevertheless, it is suggested that mobility performance can be improved by controlling in the thrust dimension.

One of the other control problems in drones is the limitations caused by mechanical and physical constraints. It has been studied on limitation-aware control such as the limitations of inputs in drones [17] and model predictive control with constrained optimization. The other standard control method that considers limitations is the control by mode switching, which is generally used in hard disc drives to switch between high-speed and high-precision modes [18].

Although experiments using actual variable pitch drones for quicker motion control have been conducted in previous research, the effects of current limitations resulting in a conservative control design have not been considered. The frequency separation method was proposed in previous research of controlling thrust dimension as a combination of the rotational speed and pitch angle [19], but interference between the pitch angle and rotational speed is not considered, and the thrust may not take the desired value if the main motor current is limited. Not only does the current limitation prevent the steady-state value from being reached, but the deterioration of the rotational speed in the transient state occurs, such as reverse responses. These effects deteriorate the drone's motion performance. Therefore, taking the thrust control by pitch angle and current into account in the design is essential.

The main contribution of this research is to propose a

Y. Naoki, S. Nagai and H. Fujimoto are with the Department of Advanced Energy, Graduate School of Frontier Sciences, The University of Tokyo, Chiba 277-8561, Japan (e-mail: naoki.yuto21@ae.k.u-tokyo.ac.jp; nagai-saka@edu.k.u-tokyo.ac.jp; fujimoto@k.u-tokyo.ac.jp).

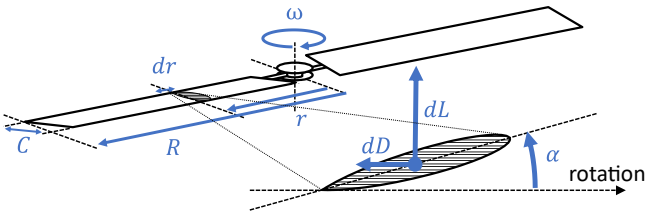

Fig. 1. Forces acting on blade element.

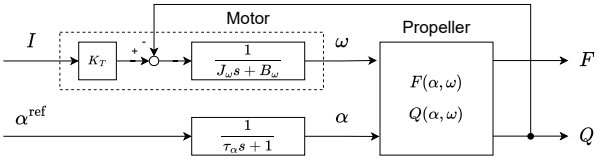

Fig. 2. Block diagram of variable pitch propeller plant model.

unified control method for variable pitch systems with motors under current limitation that improves the control range and response of the thrust while maintaining optimum efficiency in the steady state. The contributions of this manuscript can be considered as follows.

Contribution 1: A unified current-aware feedforward thrust control are designed.

Contribution 2: The thrust's response and the response's deterioration due to saturation in the thrust expansion region are improved, and the thrust tracking performance is improved by determining the command value of the pitch angle servo while using the maximum current of the main motor.

Experimental results in this paper also show that the proposed method is robust to variations in model parameters. The proposed method improves the interference problem in variable pitch propellers, which will lead to the improvements in aircraft attitude and vibration of motion.

The remainder of this paper is organized as follows. Section II formulates the problem setting of this study. The variable pitch thrust control with the mode switching algorithm is proposed in Section III. The effectiveness of the proposed method is evaluated in Section IV by both numerical simulation and test-bench experiment. Finally, the conclusions are presented in Section V.

II. Problem Formulation

In this section, the problem of improving thrust tracking performance and efficiency in variable pitch propellers is formulated. First, the variable pitch propeller system is modeled. Second, the improvement of thrust force response in the variable pitch propeller is explained. Third, the efficiency problem of changing the pitch angle is explained. Fourth, the operating point of rotational speed and pitch angle that maximize the achievable thrust is described. Fifth, the requirement in thrust control of variable pitch propellers is determined. Finally, the problem in using the conventional method when the current is limited is explained.

A. Modeling of variable pitch propeller

Forces generated by propeller blades are explained by the blade element theory. The blade element is r away from the center and has a thickness of $\mathrm{d}r$. Fig. 1 shows the forces acting on the blade element. Differential lift $\mathrm{d}L$ and differential drag $\mathrm{d}D$ can be written as

$$\mathrm{d}L = \frac{1}{2}\rho(r\omega)^2 C_L C \mathrm{d}r \tag{1}$$

$$\mathrm{d}D = \frac{1}{2}\rho(r\omega)^2 C_D C \mathrm{d}r \tag{2}$$

where ω denotes the rotational speed, ρ denotes the air density, C denotes the chord, C_L and C_D is the lift and drag coefficient respectively. Especially in drones, airspeed is almost zero in the near hovering flight condition, so the thrust F and counter torque Q generated by the propeller are equal to the sum of the lift and drag force, respectively. The lift coefficient C_L and drag coefficient C_D are dimensionless coefficients determined by the aerodynamic configuration of the propeller. These coefficients are known to be expressed in first and second order polynomials for the propeller pitch angle α respectively as

$$C_L = a_{L1}\alpha + a_{L0} \tag{3}$$

$$C_D = a_{D2}\alpha^2 + a_{D1}\alpha + a_{D0}. \tag{4}$$

The models of thrust and counter torque are calculated by integrating (1) and (2), and rewritten as

$$F = (b_{F1}\alpha + b_{F0})\,\omega^2 \tag{5}$$

$$Q = \left(b_{Q2}\alpha^2 + b_{Q1}\alpha + b_{Q0}\right)\omega^2 \tag{6}$$

where each b_{FX} and b_{QX} is constant coefficient for the model.

The equation of motion of the main motor is written as

$$T - Q = J_\omega \frac{\mathrm{d}\omega}{\mathrm{d}t} + B_\omega\omega + T_C \tag{7}$$

where B_ω denotes the viscosity coefficient, T_C denotes the coulomb friction, and T is motor torque which is proportional to the current I by a torque coefficient K_T. Also the servo motor model for the pitch angle is approximated as a first order delay with time constant τ_α as

$$\frac{\alpha}{\alpha^{\mathrm{ref}}} = \frac{1}{\tau_\alpha s + 1}. \tag{8}$$

Thus, from (5) to (8), the model of the plant can be expressed in the block diagram as shown in Fig. 2.

Here, the energy input to the propeller is written as

$$P = T\omega = Q\omega + B_\omega\omega^2 + \left(J_\omega \frac{\mathrm{d}\omega}{\mathrm{d}t} + T_C\right)\omega \tag{9}$$

and changes with the rotational speed and pitch angle.

B. Response of thrust control using variable pitch propeller

The response of the rotational speed control is determined by the inertia of propeller and torque of the main motor. When using a variable pitch mechanism, the inertia of pitch angle direction is so small compared to the motor rotational direction that the response of thrust control seems to be fast. The previous research has shown the possibility to achieve fast response with sufficiently light equipment by controlling only the pitch angle with a constant rotational speed [8].

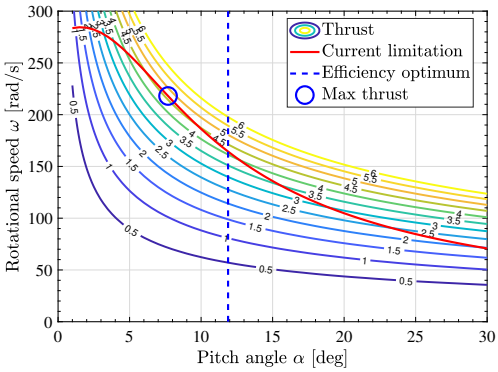

Fig. 3. Thrust map with pitch angle and rotational speed, and limitation by the current.

However, in controlling the pitch angle, as shown in the block diagram Fig. 2, the pitch angle changes the counter torque, which interferes with the rotational speed, so it is also necessary to control the motor at the same time.

C. The relationship of pitch angle and efficiency

One of the advantages of controlling both the rotational speed and the pitch angle is that it can be operated at the desired point in a steady state. The efficiency optimum operating point of the propeller is calculated as follows. If the friction term is sufficiently small in (9), the power consumption mainly depends on the counter torque. Considering general rotor efficiency, the power is expressed as the product of the thrust F and the wake velocity v produced by the rotor. Since v is proportional to the square root of F when the airspeed of the airframe is zero, it is sufficient to consider the condition that minimizes the power consumption under constant thrust to optimize efficiency. The rotational speed can be expressed by using the pitch angle and thrust from (5). By substituting (5) into (9), the steady-state power of the motor is rewritten as

$$P = \frac{b_{Q2}\alpha^2 + b_{Q1}\alpha + b_{Q0}}{(b_{F1}\alpha + b_{F0})^{\frac{3}{2}}} F^{\frac{3}{2}}. \tag{10}$$

Thus, the pitch angle α_{opt} that minimizes P is

$$\begin{aligned}\alpha_{opt} =& \frac{1}{2b_{Q2}b_{F1}} \left[-\left(4b_{Q2}b_{F0} - b_{Q1}b_{F1}\right) \right. \\ &+ \left\{ \left(4b_{Q2}b_{F0} - b_{Q1}b_{F1}\right)^2 \right. \\ &\left. \left. -4b_{Q2}b_{F1}\left(2b_{Q1}b_{F0} - 3b_{F1}b_{Q0}\right) \right\}^{\frac{1}{2}} \right], \end{aligned} \tag{11}$$

which is constant regardless of thrust F. The map by the pitch angle and rotational speed is shown in Fig. 3. The solid lines indicate the constant-thrust lines, and the red curve shows the steady-state limitation by the main motor's maximum current. The dotted line is the optimum efficiency point at calculated α_{opt}. The circle indicates the maximum thrust point.

Therefore it is practical to reduce power consumption while giving priority to response using the pitch angle transiently and then gradually change the rotational speed and return to the optimal pitch angle α_{opt}.

D. Range of achievable thrust by varying pitch angle and rotational speed

Multiple limitations must be considered when varying rotational speed and pitch angle. For electric motor propellers, there are many limitations due to the current and voltage ratings of the motor, stalling, vibration, mechanical limits of pitch angle and rotational speed. The previous studies have considered the upper limit of rotational speed due to voltage limit and the upper limit of pitch angle due to stall, but not the current [8]. However, when a larger aircraft is considered, a relatively smaller and lighter motor is used, and the problem of the current limit appears. This paper considers the limiting model of the thrust caused by the current limit.

At the upper limit of the current $I_{\max}$, the counter torque of the propeller and torque of the motor is balanced at a steady state, and the following equation holds

$$K_T I_{\max} = Q_{\max} = \left(b_{Q2}\alpha^2 + b_{Q1}\alpha + b_{Q0}\right)\omega^2. \tag{12}$$

Therefore, the thrust under a condition when the current takes the maximum current can be written as

$$F = \frac{b_{F1}\alpha + b_{F0}}{b_{Q2}\alpha^2 + b_{Q1}\alpha + b_{Q0}} K_T I_{\max}. \tag{13}$$

By calculating $\frac{\mathrm{d}F}{\mathrm{d}\alpha} = 0$, the pitch angle that generates the maximum thrust is

$$\alpha = \frac{-b_{Q2}b_{F0} + \sqrt{(b_{Q2}b_{F0})^2 - b_{Q2}b_{F1}(-b_{F1}b_{Q0} + b_{Q1}b_{F0})}}{b_{Q2}b_{F1}} \tag{14}$$

and different from (11). This shows that under a maximum torque value, the range of the thrust increases by decreasing the pitch angle and increasing the rotational speed.

E. Problem description

This paper considers the unified control method for variable pitch propellers that can achieve high tracking performance for thrust command by considering the current limit. For this purpose, the controller is designed concerning the following requirements:

Requirment 1: Increase the response of the thrust by considering the current limiting value.

Requirment 2: Move to the optimum pitch angle to increase efficiency at a steady state after the thrust is tracked.

Requirment 3: Reach to the maximum thrust by varying pitch angle and rotational speed command values.

In meeting these requirements, the tracking performance and responsiveness of the thrust control, which are directly related to the tracking performance of the drone, are designed as a priority, and the efficiency is considered after the tracking performance has been satisfied.

F. Appplication of conventional frequency separation method to variable pitch thrust control

In the conventional approach, the controller is designed by frequency separation method, which can control thrust by separating the thrust command by a filter into high band component for pitch angle and the low band component for

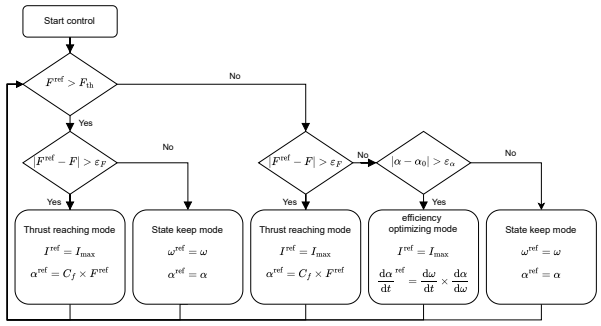

Fig. 4. The whole flow of the proposed method.

rotational speed [19]. By linearizing (5) and approximating the main motor and pitch angle servo with a first-order system of τ_α and τ_ω, the plant is written as

$$\Delta F = \frac{a}{\tau_\alpha s + 1}\Delta\alpha^* + \frac{b}{\tau_\omega s + 1}\Delta\omega^* \tag{15}$$

where a and b are linearized coefficients of thrust model. Then the frequency separation controller is designed as

$$\Delta\alpha^* = \frac{\tau_\alpha s + 1}{a}\left(k_\alpha + k_\omega \frac{\tau_{fs} s}{\tau_{fs} s + 1}\right)\frac{1}{\tau_F s + 1}\Delta F^{\mathrm{ref}} \tag{16}$$

$$\Delta\omega^* = \frac{\tau_\omega s + 1}{b}\frac{k_\omega}{\tau_{fs} s + 1}\frac{1}{\tau_F s + 1}\Delta F^{\mathrm{ref}} \tag{17}$$

where τ_{fs} is filter parameter, k_ω and k_α are steady state allocation parameter, so that it can follow the thrust with first-order system of τ_F while moving to any operating point.

However, this method requires conservative design with respect to current limits, and there is a problem of undershoot response if current is not taken into account. Therefore the *Requirment* 1 and 3 are not satisfied at the same time.

III. Maximum current variable pitch thrust control with switching of control laws

In this section, a control method that can achieve all the requiements by switchng control modes in different current range is described. It can be applied as a feed-forward control method for any thrust command value by switching modes. The thrust control is inside of the attitude and position control. The strategy is as follows. First, the rotational speed and pitch angle state are moved to reach the target thrust using the maximum current of the main motor. Then after the thrust is reached to the target, if the thrust is within the reachable range at the optimum efficiency pitch angle, efficiency is improved by returning to the optimum efficiency pitch angle. Finally,the states are controlled to keep the steady-state value. The flow of switching modes is shown in Fig. 4.

A. Commanded thrust reaching mode

If the thrust is far enough from the reference, the pitch angle is changed while applying the maximum current to reach the reference thrust quickly. The concept of controller design using the maximum current was proposed in [20]. The model of thrust with respect to pitch angle and current is considered. Substituting the model of counter torque expressed by (6) into the model of the motor and linearizing it concerning the pitch angle and rotational speed and Laplace transforming, the rotational speed can be calculated as the sum of the pitch angle and the current first-order systems as

$$\omega = -\frac{K_{Q\alpha}}{J_\omega s + B_\omega + K_{Q\omega}}\alpha + \frac{K_T}{J_\omega s + B_\omega + K_{Q\omega}} I \tag{18}$$

where $K_{Q\omega}, K_{Q\alpha}$ are the respective coefficients of the counter torque model (6) linearized by pitch angle and rotational speed. By Linearizing (5) and substituting (18), the linearlized thrust model can be rewritten as

$$\begin{aligned} F &= K_{F\omega}\omega + K_{F\alpha}\alpha \\ &= K_\alpha \frac{s - z_\alpha}{s + p_\alpha}\alpha + K_I \frac{1}{s + p_\alpha} I \end{aligned} \tag{19}$$

where z_α, p_α is the zero and pole of the system as a positive value. (19) shows that the transfer function from the pitch angle to the thrust has an unstable zero. The qualitative explanation for the unstable zero is that the system has the characteristic of temporarily increasing direct thrust as the pitch angle increases but decreasing thrust as the rotational speed decreases. A controller is designed for this model. Setting the current command value as the maximum value, the effect of the current on the thrust is fixed in the first-order system. First, the thrust command value is converted to a pitch angle command. If the thrust command value is greater than the current thrust, the pitch angle command value is determined as the pitch angle that results in the maximum counter torque under the target thrust condition. The pitch angle command is calculated from thrust command F^{ref} by solving (5) and (6) substituting $F = F^{\mathrm{ref}}$ and $Q = K_T I_{\max}$. If the thrust command is smaller than the present thrust, the pitch angle command is set to zero. The pitch angle controller C_{reach} is designed by pole-zero cancellation.

$$C_{reach} = \frac{\frac{1}{p_\alpha} s + 1}{\tau_f s + 1} \tag{20}$$

B. Efficiency optimizing mode

If the thrust is close enough to the reference, the pitch angle is controlled to return to the optimum efficiency pitch angle while maintaining the thrust. It is assumed that the maximum current is also used for the input in this mode. When a certain thrust F_{const} is desired output which satisfies (5) with the change of the rotational speed ω and pitch angel α, the below equation can be derived as

$$\frac{\mathrm{d}\alpha}{\mathrm{d}\omega} = \frac{F_{\mathrm{const}}}{b_{F1}}(-2\omega^{-3}). \tag{21}$$

Assuming that the rotational speed ω is measurable, the reference of the pitch angle velocity can be calculated as the product of (21) and differential value of ω.

C. Rotational speed control mode

After the pitch angle reaches the optimum pitch angle, the rotational speed and pitch angle state are controlled to keep the steady state. It is necessary to prevent chattering

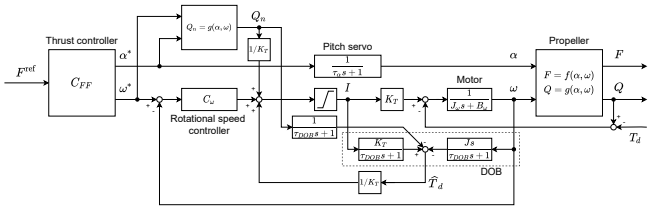

Fig. 5. Rotational speed based thrust control system used in this study.

due to external disturbances when the thrust command value is constant. In this step, the current has room for counter torque compensation by an observer, so a regulator with a disturbance observer is designed as rotational speed control. The configuration of Rotational speed control mode is shown in Fig. 5. The command values for rotational speed and pitch angle in this control step can be calculated from the command value thrust and the steady-state pitch angle. The configuration is the same as the control shown in Fig. 5

D. Mode switching law

The flow of switching modes is shown in Fig. 4. Here, ε_F and ε_α are acceptable errors values. In particular, in the steady-state current non-saturated region where $F^{\mathrm{ref}} <= F_{\mathrm{th}}$, efficiency optimizing mode is used to return to the efficiency optimum pitch angle. On the other hand, in the steady state current saturated region where $F^{\mathrm{ref}} > F_{\mathrm{th}}$, since the purpose is to extend thrust, the efficiency optimizing mode is not used. Here, F_{th} is the boundary thrust between saturated and non-saturated regions and corresponds to the maximum thrust when the optimum pitch angle is taken.

As an implementation issue, the thrust value for a criterion for switching the mode cannot be directly measured since drones do not have thrust meters. The thrust value is calculated by (5) and (6) using measured state ω and α. However, because the measured rotational speed includes noise, a low pass filter is applied to the measurement for calculation. ε_F and ε_α added to threshold values for switching also work as dead-zones to avoid chattering.

IV. Simulation and Experimental Validation

In this section, the approach in Section 3 is applied to variable pitch system. The behavior of the proposed method at multiple thrust conditions is confirmed through simulations. The experimental results demonstrate the performance improvement.

A. Setup

The experimental setup of the variable pitch propeller system is shown in Fig. 6. The load cell, encoder, and current sensor measure the thrust, rotational speed, and motor current. The propeller radius is $0.2\,\mathrm{m}$. Since the actual pitch angle cannnot be directly measured, the calculated value from servo model and control input is taken as a measurement. The pitch angle model is identified by measureing the thrust response by changing the pitch angle. The motor parameters J_ω, B_ω and

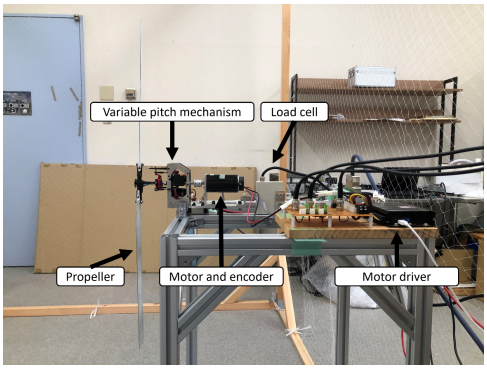

Fig. 6. Experimental setup of variable pitch propeller system. The 25cm length propeller blades are rotated by the main motor, and the pitch angle is changed by variable pitch mechanism.

TABLE I
Motor Parameters

Parameter	Value
Inertia moment of propeller J_ω	$1.4 \times 10^{-2}\,\mathrm{kgm^2}$
Viscosity coefficient of motor B_ω	$2.3 \times 10^{-6}\,\mathrm{N\,m\,s\,rad^{-1}}$
Coulomb friction of motor T_C	$2.4 \times 10^{-3}\,\mathrm{N\,m}$
Torque constant K_T	$30.2 \times 10^{-3}\,\mathrm{N\,m\,A^{-1}}$
Max. continuous current $I_{\max}$	$4\,\mathrm{A}$

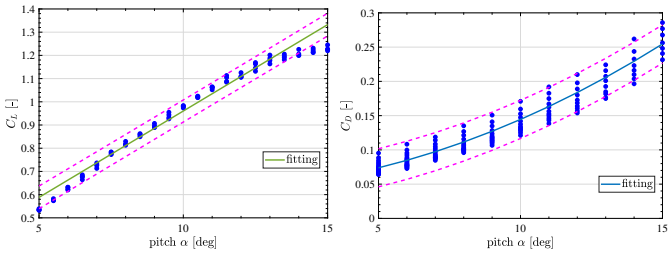

Fig. 7. Propeller model. Blue dots shows mesurments in multiple rotational speed and pitch angle, the dotted lines show the 95% confidence intervals. (a) Relationship between pitch angle α and lift coefficient C_L. (b) Relationship between pitch angle α and drag coefficient C_D.

TABLE II
Propeller Parameters

Parameter			Parameter		
b_{F1}	b_{F0}		1.45×10^{-5}	5.82×10^{-6}	
b_{Q2}	b_{Q1}	b_{Q0}	3.16×10^{-8}	9.00×10^{-8}	1.70×10^{-6}

T_C are identified by the method based on [21] as shown in Table I. The propeller parameters C_L, C_D are measured and fitted to (3) and (4). The measurement and fitted results are shown in Fig. 7 and Table II.

B. Simulation of mode variation in the proposed method

The control method of mode switching is verified by simulation conducted under four thrust command $\Delta F^{\mathrm{ref}} = 0.2\,\mathrm{N}$, $0.5\,\mathrm{N}$, $0.9\,\mathrm{N}$ and $-0.3\,\mathrm{N}$ in which the switching conditions are varied. The simulation conditions are based on the setup,

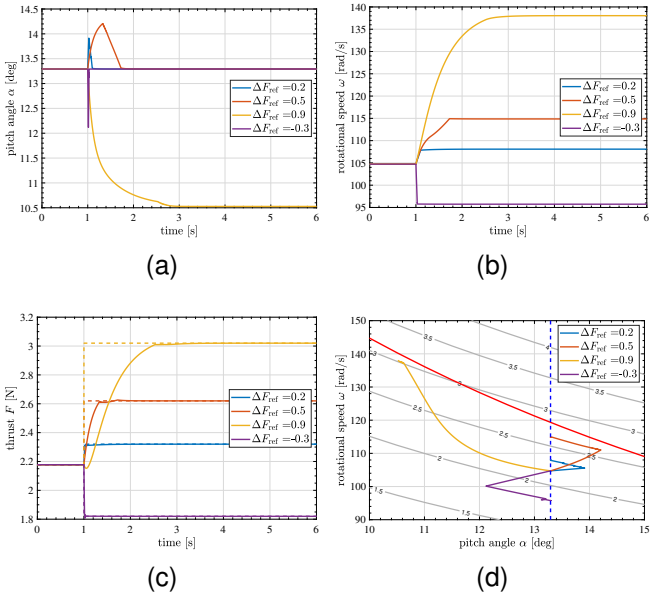

Fig. 8. Simulation results of four cases. (a) α, (b) ω, (c) F, (d) Trajectory map

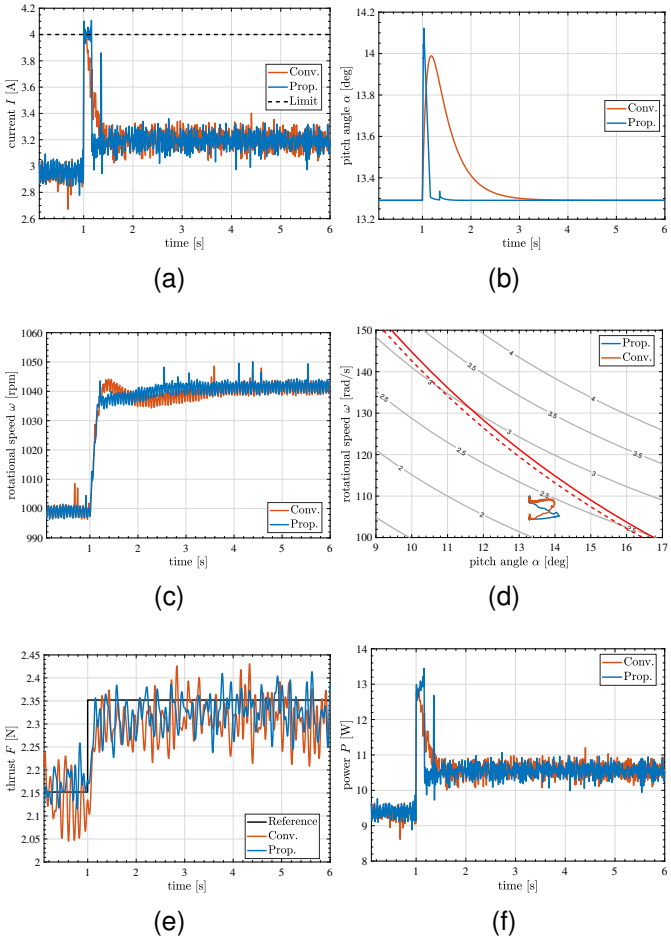

Fig. 9. Experimental result. ΔF^{ref} =0.2 N (a) I, (b) α, (c)ω, (d) Trajectory map, (e) F, (f) P

and the operating point is set as $\omega_0 = 1000\,\mathrm{rpm}$ and $\alpha_0 = 13.3\,\mathrm{deg}$. This is hypothetical condition of hovering for 0.9 kg quadrotor-UAV. The situation of step thrust corresponds to a step change in weight or acceleration. The results in Fig. 8 show the different switching behavior under different step widths. The trajectory changes depending on the relationship between the thrust contour of the reference and the counter torque saturation region, where the counter torque is balanced with the maximum torque that can be output by the steady-state current, represented by the red line on the map in Fig. 8d. First, in the case of small thrust step width ΔF^{ref} =0.2 N, the thrust reaches around the command value by the thrust reaching mode before getting to the counter torque saturation region. The state quickly transitions to the efficiency optimizing mode. Next, in the case of medium thrust step width ΔF^{ref} =0.5 N, the state reaches the counter torque saturation region in the thrust reaching mode and switches to the efficiency optimizing mode after the thrust is sufficiently settled. Third, in the case of large thrust step width ΔF^{ref} =0.9 N, the pitch angle is reduced in the thrust reaching mode, and the efficiency optimizing mode is not used. Fourth, if the thrust change is negative ΔF^{ref} =−0.3 N, the target thrust is achieved by the negative change in rotational speed and pitch angle, then returns to the optimum pitch angle.

C. Experimental validation of the thrust control using maximum current by mode switching control

The experiment compares the proposal to the conventional method mentioned in (16), (17). The conditions are the same as the simulation, with two different step references $\Delta F^{\mathrm{ref}} =$ 0.2 N and 0.9 N. The simulation results show that the medium thrust step width is closer to the current limitation region than the small step width, and a condition advantageous to the proposed method. In addition, the negative thrust step case results in the opposite transition to that of the small step width case. Therefore the two cases are omitted from the experimental results. Note that the measurement is filtered by $20\,\mathrm{rad/s}$ zero-phase filter for the current, rotational speed, and motor power and $10\,\mathrm{rad/s}$ zero-phase filter for thrust. The error in thrust up to 5 s and the average motor power and efficiency at steady state (after 5 s) for the case of ΔF^{ref} =0.2 N are shown in Table III. The results of small thrust step width ΔF^{ref} =0.2 N are shown in Fig. 9. Fig. 9a and Fig. 9b show that the proposed method can settle the current and the pitch angle states faster than the conventional method of frequency separation. Fig. 9c shows that it takes more time in rotational speed with conventional method because of the settling time of pitch angle. As shown in Fig. 9e, the difference in the thrust appears to be very small, but since the maximum current is used in the transient, the proposed method gives the best results as the integrated value of the squared error of thrust

TABLE III
PERFORMANCE COMPARISON IN SMALL STEP CONDITION

method	$\int \lvert F^{\mathrm{ref}} - F\rvert^2 dt$	$\bar{P}$	$\bar{P}/\bar{F}$
Conv.	$0.033\,\mathrm{N}^2$	10.5 W	$4.57\,\mathrm{W\,N^{-1}}$
Prop.	$0.015\,\mathrm{N}^2$	10.5 W	$4.54\,\mathrm{W\,N^{-1}}$

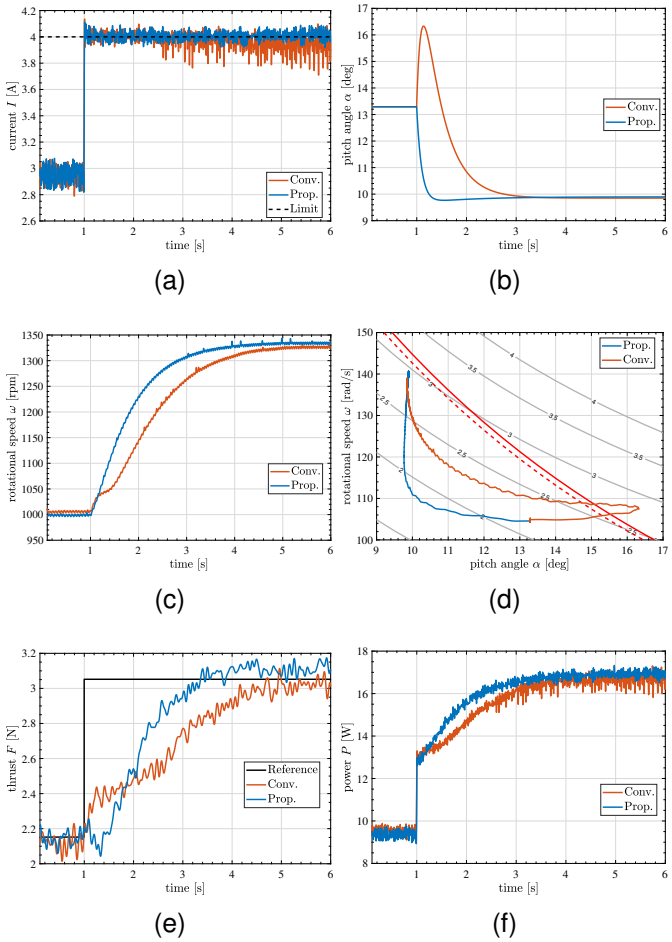

Fig. 10. Experimental result. ΔF^{ref} =0.9 N (a) I, (b) α, (c) ω, (d) Trajectory map, (e) F, (f) P

shown in Table III. In addition, in the required power of the propeller shown in Fig. 9f, the power is the same in both methods because the final steady state is matched. This shows that the proposed method can use the same efficient state as the frequency separation. The result of large thrust step width $\Delta F^{\mathrm{ref}} = 0.9\,\mathrm{N}$ are shown in Fig. 10. In the conventional control, the state shown in Fig. 10d has exceeded the torque saturation region, and it has a delay in the rotational speed as shown in Fig. 10c. The final value of power matches as shown in Fig. 10f. The proposed method does not cause this problem and improves the response as shown in Fig. 10e and the settling time improves about 1 s.

In both cases, there is a steady-state error in the thrust value. This is because the thrust is controlled in a feed-forward using a model. The errors in the thrust coefficients shown in Fig. 7a affect the thrust error performance.

D. Discussions on Parameter Variations

The method assumes that propeller model (C_L, C_D) and motor model (J_ω, B_ω, T_c) are accurate. The influences of errors in the models are discussed in this section.

The propeller model influences command value generation in the thrust reaching mode and the efficiency optimizing mode. In the rotational speed control mode, the influence is insignificant due to the disturbance observer. In the thrust reach mode, the propeller model is used in calculating the pitch angle command from the thrust reference. In particular, if the counter torque model is calculated to be smaller than the actual value, the desired thrust may not be reached, and the switching may not converge. Thus, a margin of counter torque needs to be added in calculating the command value. In the experiment, the margin was set with reference to the variance shown in Fig. 7 In the efficiency optimizing mode, propeller model errors may lead to significant thrust variations. However, if the amount of variation is small enough, it can be absorbed by the allowable limit of error.

TABLE IV
NOMINAL MOTOR PARAMETER WITH ERROR

Parameter	Value
Nominal inertia with error $J_{\omega n}$	$6.9 \times 10^{-3}\,\mathrm{km}^2$
Nominal viscosity coefficient with error $B_{\omega n}$	$5.0 \times 10^{-6}\,\mathrm{N\,m\,A^{-1}}$

The error of the motor model affects the trajectory of the states because the motor model is used to design the controller in the thrust reaching mode and generate commands in the pitch angle optimizing mode. First, the effect in the thrust reach mode is theoretically considered. The error is discussed using the linearized plant model as the design in (19). The first term of (19) ΔF_α, which is the variation of thrust due to pitch angle without model error can be expressed as,

$$\Delta F_\alpha = P_\alpha C_\alpha \Delta\alpha^{\mathrm{ref}} \tag{22}$$

$$= P_\alpha \times \left(\frac{s - p_\alpha}{-p_\alpha} \times \frac{1}{\tau_f s + 1} \right) \times \Delta\alpha^{\mathrm{ref}} \tag{23}$$

where the pole p_α of the transfer function from the linearized pitch angle to the thrust as

$$p_\alpha = -\frac{J_\omega + K_{Q\omega}}{B_\omega}. \tag{24}$$

Thus, the effect of theoretical model error is

$$\Delta F'_\alpha = P_\alpha C'_\alpha \Delta\alpha^{\mathrm{ref}} \tag{25}$$

$$= \Delta F_\alpha + P_\alpha \times \left(s \left(\frac{1}{p_\alpha} - \frac{1}{p'_\alpha} \right) \times \frac{1}{\tau_f s + 1} \right) \times \Delta\alpha^{\mathrm{ref}} \tag{26}$$

where p'_α is a pole of the nominal model transfer function. Thus, the theoretical error has a high pass characteristics and does not remain the steady-state error.

On the other hand, the effects of model error in the pitch angle optimizing mode are dominated by the effects of the thrust and lift coefficients because the sign of the pitch angle change in optimizing mode does not change even if inertia changes and the constant thrust condition expressed by (21) is satisfied.

The effect of this motor model error can be verified by experiments. The values by a single measurement are used as nominal values shown in Table IV while used actual values in Table I are measured by multiple measurements. Experimental results are shown in Fig. 11. The experimental results show that the pitch angle does not increase when there is a model

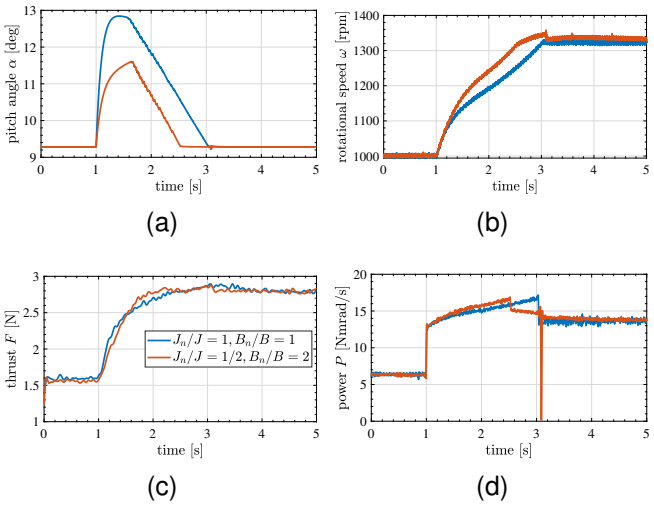

Fig. 11. experimental result. $\Delta F^{\mathrm{ref}} = 1\,\mathrm{N}$ (a) α, (b) ω, (c) F, (d) P.

error compared to the case without the error. Instead, the desired thrust is achieved by increasing the rotational speed. From Fig. 11a, the pitch angle does not change significantly because the pitch angle controller is designed slowly, assuming that the inertia is small and the rotational speed can be easily increased in the thrust reach mode. In addition, performance is evaluated with and without modeling error in the result. The result is numerically evaluated by the square error of the thrust and the time integration of the motor power. The squared error of the thrust with model error is higher as $0.31\,\mathrm{N^2s}$ than that without model error as $0.28\,\mathrm{N^2s}$ even though the energy consumption is lower as $66.8\,\mathrm{J}$ with nominal error compared to $67.2\,\mathrm{J}$ without the model error. Since this method emphasizes the response of the thrust, it is desirable to use an accurate model. However, it is experimentally verified that the method has lobustness for motor model error.

V. CONCLUSION

A feed-forward control method in which the maximum current is used to control the thrust by the pitch angle and rotational speed under a current limit is proposed for a variable pitch system. The proposed variable pitch thrust control is designed to switch control laws according to the desired thrust and state of rotational speed and pitch angle. The response of each control law is improved by designing the pitch angle control according to the maximum value of the current used for the change in the rotational speed. Furthermore, the pitch angle with optimum efficiency and maximum thrust is calculated from the model, and the control method to extend the achievable thrust and improve efficiency is unified by switching the command value. Simulations demonstrated that the system is adaptable to arbitrary thrust, and improvement of thrust tracking performance and efficiency is verified by applying it to experimental systems. The proposed method is a feed-forward control of thrust, and a steady-state error of thrust occurs when there is an error in the thrust coefficient. Model correction of the thrust coefficient, such as in the presence of wind, is a future work.

REFERENCES

[1] K. Nonami, "Drone technology, cutting-edge drone business, and future prospects." *Journal of Robotics and Mechatronics*, vol. 28, no. 3, pp. 262–272, 2016.

[2] K. Yokota and H. Fujimoto, "Aerodynamic force control for tilt-wing evtol using airflow vector estimation," *IEEE Transactions on Transportation Electrification*, vol. 8, no. 4, pp. 4163–4172, 2022.

[3] J. Lee, K. K. Leang, and W. Yim, "Design and control of a fully-actuated hexrotor for aerial manipulation applications," *Journal of Mechanisms and Robotics*, vol. 10, no. 4, 2018.

[4] K. Takishima and K. Sakai, "Design Method for Ultralightweight Motor Using Magnetic Resonance Coupling and its Characteristics," *IEEJ Journal of Industry Applications*, 2021.

[5] F. Yacef, N. Rizoug, O. Bouhali, and M. Hamerlain, "Optimization of energy consumption for quadrotor uav," in *Proceedings of the International Micro Air Vehicle Conference and Flight Competition (IMAV), Toulouse, France*, 2017, pp. 18–21.

[6] N. Kobayashi, H. Fujimoto, Y. Hori, H. Kobayashi, and A. Nishizawa, "A study of Range Extension Control System by Optimization of Motor Torque and Propeller Pitch Angle for Electric Airplane," *Technical Meeting on Industrial Instrumentation and Control*, vol. 2013, no. 89, pp. 31–36, 2013.

[7] Y. Xiang, H. Fujimoto, Y. Hori, Y. Watanabe, and K. Suzuki, "Proposal of Regeneration Power Control System by Optimization of Propeller Pitch Angle and Revolution Speed for Electric Airplanes," *IEE of Japan Technical Meeting Record*, vol. 15, no. 49, pp. 121–126, 2015.

[8] M. Cutler and J. P. How, "Analysis and control of a variable-pitch quadrotor for agile flight," *Journal of Dynamic Systems, Measurement and Control, Transactions of the ASME*, vol. 137, no. 10, 2015.

[9] V. M. Arellano-Quintana, E. A. Merchan-Cruz, and A. Franchi, "A novel experimental model and a drag-optimal allocation method for variable-pitch propellers in multirotors," *IEEE Access*, vol. 6, pp. 68 155–68 168, 2018.

[10] Z. Wang, R. Groß, and S. Zhao, "Control of centrally-powered variable pitch propeller quadcopters subject to propeller faults," *Aerospace Science and Technology*, vol. 120, p. 107245, 2022.

[11] S. Komizunai, M. Uraoka, and A. Konno, "Development and Thrust Response Evaluation of a Variable Pitch Propeller Quad Tilt-rotor Drone," *Transactions of the Society of Instrument and Control Engineers*, vol. 6, no. 49, pp. 310–316, 2020.

[12] K. Kawasaki, K. O. M. Zhao, and M. Inaba, "MUWA: Multi-field universal wheel for air-land vehicle with quad variable-pitch propellers," *IEEE/RSJ International Conference on Intelligent Robots and Systems*, pp. 1880–1885, 2013.

[13] N. Gupta, M. Kothari, and Abhishek, "Flight dynamics and nonlinear control design for variable-pitch quadrotors," in *2016 American Control Conference (ACC)*, 2016, pp. 3150–3155.

[14] A. K. Shastry, M. T. Bhargavapuri, M. Kothari, and S. R. Sahoo, "Quaternion based adaptive control for package delivery using variable-pitch quadrotors," in *2018 Indian Control Conference (ICC)*, 2018, pp. 340–345.

[15] A. B. Krishna and M. Kothari, "Robust geometric trajectory tracking control of a variable-pitch quadrotor," *Journal of Guidance, Control, and Dynamics*, vol. 45, no. 5, pp. 902–920, 2022.

[16] M. Bangura and R. Mahony, "Thrust control for multirotor aerial vehicles," *IEEE Transactions on Robotics*, vol. 33, no. 2, pp. 390–405, 2017.

[17] X. Shao, G. Sun, W. Yao, J. Liu, and L. Wu, "Adaptive sliding mode control for quadrotor uavs with input saturation," *IEEE/ASME Transactions on Mechatronics*, vol. 27, no. 3, pp. 1498–1509, 2022.

[18] T. Yamaguchi, H. Numasato, and H. Hirai, "A mode-switching control for motion control and its application to disk drives: design of optimal mode-switching conditions," *IEEE/ASME Transactions on Mechatronics*, vol. 3, no. 3, pp. 202–209, 1998.

[19] Y. Naoki, S. Nagai, and H. Fujimoto, "Basic study on thrust control using frequency separation in variable pitch propeller mechanisms for response and efficiency improvement of drones," in *the 8th IEEJ international workshop on Sensing, Actuation, Motion Control, and Optimization*, 2022.

[20] Y. Naoki, K. Yokota, S. Nagai, and H. Fujimoto, "Achievable thrust expansion control at current saturation of variable-pitch propeller for drones," *IFAC-PapersOnLine*, vol. 55, no. 27, pp. 247–252, 2022, 9th IFAC Symposium on Mechatronic Systems MECHATRONICS 2022.

[21] K. Yokota and H. Fujimoto, "Pitch angle control by regenerative air brake for electric aircraft," *IEEJ Journal of Industry Applications*, vol. 11, no. 2, pp. 308–316, 2022.

Yuto Naoki received the B.E. degree from the Department of Electrical and Electronic Engineering, The University of Tokyo, Chiba, Japan, in 2022. He is currently pursuing the M.S. degree with the Department of Advanced Energy, Graduate School of Frontier Sciences, The University of Tokyo.

His research interests includes multirotor control.

Mr. Naoki is a Student Member of the Institute of Electrical Engineers of Japan.

Sakahisa Nagai Sakahisa Nagai received the B.E., M. E., and Ph. D. degrees in electrical and computer engineering from the Department of Electrical and Computer Engineering, Yokohama National University, Kanagawa, Japan, in 2014, 2016, and 2019, respectively. Since 2019, he has been a project Assistant Professor with the Graduate School of Frontier Sciences, The University of Tokyo, Kashiwa, Japan. His research intersts include sensorless actuation, motion control, wireless power transfer, and power electronics. Dr. Nagai is a Member of IEE of Japan.

Hiroshi Fujimoto Hiroshi Fujimoto received the Ph.D. degree in the Department of Electrical Engineering from the University of Tokyo in 2001.

In 2001, he joined the Department of Electrical Engineering, Nagaoka University of Technology, Nigata, Japan, as a research associate. From 2002 to 2003, he was a visiting scholar in the School of Mechanical Engineering, Purdue University, U.S.A. In 2004, he joined the Department of Electrical and Computer Engineering, Yokohama National University, Yokohama, Japan, as a lecturer and he became an associate professor in 2005. He had been an associate professor of the University of Tokyo from 2010 to 2020 and became a professor from year 2021.

He received the Best Paper Awards from the IEEE Transactions on Industrial Electronics in 2001 and 2013, Isao Takahashi Power Electronics Award in 2010, Best Author Prize of SICE in 2010, The Nagamori Grand Award in 2016, and First Prize Paper Award IEEE Transactions on Power Electronics in 2016.

His interests are in control engineering, motion control, nano-scale servo systems, electric vehicle control, motor drive, visual servoing, and wireless motors. Dr. Fujimoto is a senior member of IEE of Japan and IEEE. He is also a member of the Society of Instrument and Control Engineers, the Robotics Society of Japan, and the Society of Automotive Engineers of Japan.